ChemPubSoc Europe
DOI: 10.1002/chem.201xxxxxx
CHEMISTRY A European Journal Full Paper

chiral Zn(II) cages

# Trinuclear cage-like Zn(II) macrocyclic complexes: enantiomeric recognition and gas adsorption properties.

Jan Janczak[a], Daniel Prochowicz[b], Janusz Lewiński[b], David Fairen-Jimenez[c], Tomasz Bereta [d] and Jerzy Lisowski*[d]

**Abstract:** Three zinc(II) ions in combination with two units of enantiopure 3+3 triphenolic Schiff base macrocycles **1**, **2**, **3** or **4** form cage-like chiral complexes. The formation of these complexes is accompanied by the enantioselective self-recognition of chiral macrocyclic units. The X-ray crystal structures of these tricuclear complexes show hollow metal-organic molecules. In some crystal forms, these barrel-shaped complexes are arranged in a window-to-window fashion which results in formation of 1-D channels and combination of intrinsic porosity with extrinsic porosity. The microporous nature of the [$Zn_3$**1**$_2$] complex is reflected in its $N_2$, Ar, $H_2$ and $CO_2$ adsorption properties. The $N_2$ and Ar adsorption isotherms showed pressure gating behaviour which is without precedent for any noncovalent porous material. The comparison of the structures of the [$Zn_3$**1**$_2$] and [$Zn_3$**3**$_2$] complexes with that of the free macrocycle $H_3$**1** reveals a striking structural similarity. In the latter compound two macrocyclic units stitched together by hydrogen bonds form a cage very similar to that formed by two macrocyclic units stitched together by Zn(II) ions. This structural similarity is manifested also by the gas adsorption properties of the free $H_3$**1** macrocycle. Recrystallization of [$Zn_3$**1**$_2$] in the presence of racemic 2-butanol results in enantioselective binding of the (*S*)-2-butanol inside the cage via coordination to one of Zn(II) ions.

## Introduction

The synthesis of robust porous networks that can be achieved by noncovalent-driven self-assembly processes has attracted special attention in recent years.[1] Although a variety of robust noncovalent porous materials (NPMs) derived from discrete organic molecules[2] and molecular metal complexes[3] have been prepared, the synthesis of homochiral NPMs is highly challenging. To date, a few examples including mononuclear,[4] dinuclear[5] and high-nuclearity metallamacrocycle[6] chiral systems with permanent porosity have been reported. Such homochiral porous molecular assemblies opens the way for guest-responsive materials[7] that can compete with classical MOFs as highly selective adsorbents exhibiting enantioselective and gas sorption properties.[4,5]

Enantiopure 3+3 macrocycles derived from *1,2-trans*-diaminocyclohexane and aromatic dialdehydes are versatile chiral ligands for coordination of various metal ions.[8-10]. Similar 3+3 macrocycle derived from 1,2-diaminobenzene was used to obtain metal-macrocycle frameworks with enantiomeric pairs of guest binding pockets.[11] We have recently shown that the triphenolic 3+3 Schiff base macrocycle derived from *1,2-trans*-diaminocyclohexane, $H_3$**1,** or its enantiomer $H_3$**2,** form trinuclear Zn(II) complexes. In these compounds two deprotonated macrocyclic units are connected by metal ions effectively forming a cage-like molecule [$Zn_3$**1**$_2$] with the interior occupied by solvent molecules (Scheme 1).[8] In that respect [$Zn_3$**1**$_2$] resembles larger metal-seamed nanocapsules based on two pyrogallol[4]arenes connected by Zn(II) ions.[12] Both complexes belong to a class of hollow molecules constructed from metal ions and organic fragments, referred to as metal-organic containers, metallo-supramolecular capsules or metallocavitands.[12-14] These compounds attract increasing attention as host for various guest molecules. Although the rather small volume of the interior of [$Zn_3L_2$] (L = **1** – **4**) complexes limits the number of potential organic guests, the container-like structure of these complexes suggests the possibility of gas capture based on intrinsic microporosity after removal of solvent guest molecules.

[a] *Prof. J. Janczak*
*Institute of Low Temperature and Structure Research, Polish Academy of Sciences, P. O. Box 1410, 50-950, Wrocław (Poland)*

[b] *Dr. D. Prochowicz, Prof. J. Lewiński*
*Institute of Physical Chemistry, Polish Academy of Sciences, Kasprzaka 44/52, 01-224 Warsaw (Poland)*

[c] *Dr. D. Fairen-Jimenez*
*Department of Chemical Engineering & Biotechnology, University of Cambridge, Pembroke Street, Cambridge CB2 3RA (United Kingdom).*

[d] *T. Bereta, Prof. J. Lisowski*
*Department of Chemistry, University of Wrocław, F. Joliot-Curie 14, 50-383 Wrocław (Poland), E-Mail: jerzy.lisowski@chem.uni.wroc.pl*

*Supporting information for this article is available on the WWW under http://www.chemeurj.org/ or from the author.*

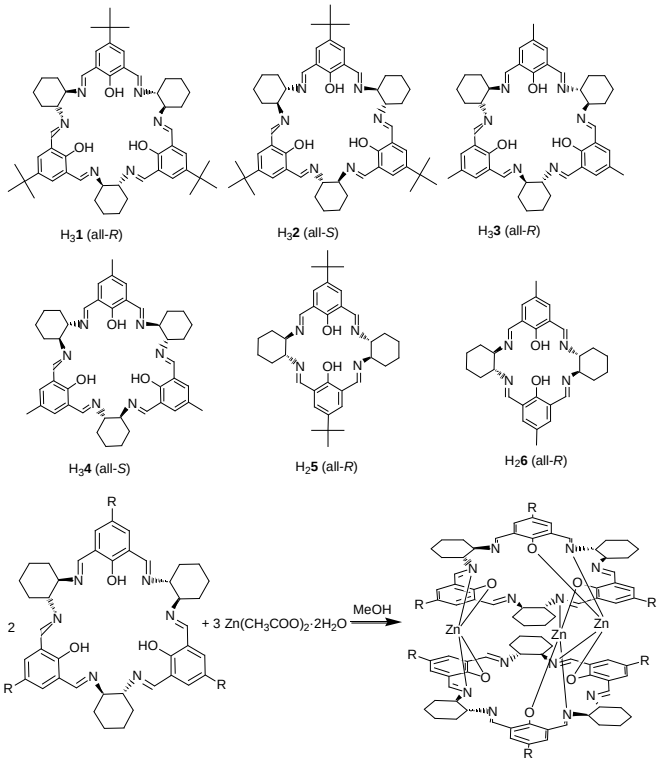


**Scheme 1**. Schematic representation of the protonated forms of the 3+3 and 2+2 macrocycles and the formation of the trinuclear container-like $[Zn_3L_2]$ complexes.

Herein, we report a comprehensive study on the synthesis, molecular and crystal structures, and gas adsorption properties of a series of cage-like homochiral complexes derived from enantiopure 3+3 triphenolic Schiff base macrocycles. We also show that the formation of $[Zn_3L_2]$ complexes is accompanied by enantiomeric self-recognition. Enantiomeric self-recognition, called also homochiral self-sorting is a kind of self-sorting phenomena that attracts increasing attention in various areas of chemistry, including inorganic chemistry.[15] In particular, the coordination of chiral ligands to a central metal ion accompanied by self-sorting of enantiomers is observed only in rare cases.[16] Here demonstrate that such self-sorting of enantiomers of macrocyclic ligand is operating also in the case of trinuclear complexes. We also demonstrate that enantiomeric recognition plays a role in binding of chiral alcohols, such as 2-butanol, by $[Zn_3L_2]$ complexes.

## Results and Discussion

### Synthesis of the $[Zn_3L_2]$ and $[Zn_2L']$ complexes; enantiomeric-self recognition of the 3+3 macrocyclic ligands

Trinuclear $[Zn_3L_2]$ (L = **1** – **4**) complexes can be easily obtained in methanol starting from the appropriate 3+3 Schiff base macrocycles $H_3L$ and zinc(II) acetate used in a 2:3 ratio. In the case of the new derivatives $[Zn_3\mathbf{3}_2]$ and $[Zn_3\mathbf{4}_2]$ with methyl substituents on the aromatic ring the yields (34%) are lower in comparison with the derivatives $[Zn_3\mathbf{1}_2]$ and $[Zn_3\mathbf{2}_2]$, which possess the *tert*-butyl substituents. As we have reported previously,[8] the $[Zn_3\mathbf{1}_2]$ complex can be also obtained in a direct template condensation of (*1R),(2R)-trans*-diaminocyclohexane and 2,6-diformyl-4-*tert*-butyl-phenol, provided 0.5 equivalent of Zn(II) acetate per 1 equivalent of diamine and 1 equivalent of dialdehyde is used. On the other hand, the application of 1 equivalent of Zn(II) template leads to the formation of dinuclear Zn(II) complex $[Zn_2\mathbf{5}(AcO)_2]$ of a smaller 2+2 macrocycle. Such a situation corresponds to a unique control over the size of the formed macrocycle by the amount of the used template ion (Scheme 2). In the case of the new derivative of 4-methyl-2,6-diformylphenol this selectivity is less pronounced; while the application of 1 equivalent of Zn(II) leads selectively to a dinuclear complex $[Zn_2\mathbf{6}(AcO)_2]$ of a 2+2 macrocycle (51% isolated yield), the application of 0.5 equivalent of Zn(II) in a template synthesis leads to a mixture of trinuclear Zn(II) complex of a 3+3 macrocycle $[Zn_3\mathbf{3}_2]$, dinuclear Zn(II) complex of a 2+2 macrocycle $[Zn_2\mathbf{6}(AcO)_2]$ and the free 3+3 macrocycle $H_3\mathbf{3}$. These products can be easily distinguished by their NMR spectra, those of $[Zn_3\mathbf{3}_2]$ and $H_3\mathbf{3}$ indicate $C_3$ symmetry, in contrast to the spectrum of $[Zn_2\mathbf{6}(AcO)_2]$ indicating $D_2$ symmetry (Figures S1-S3). The selective formation of $[Zn_3L_2]$ complexes seems to be governed by factors such as solubility and formation of kinetic products. In the case of $[Zn_3\mathbf{3}_2]$ (or $[Zn_3\mathbf{4}_2]$) complex the influence of these factors can be illustrated by the outcome of the reaction of 2 equivalents of 3+3 macrocycle and 3 equivalents of Zn(II) acetate in methanol or chloroform. While in the former solvent the trinuclear Zn(II) complex can be obtained, in the latter solvent 1.5 equivalents of dinuclear 2+2 complex $[Zn_2\mathbf{6}(AcO)_2]$ was formed and 1 equivalent of the free 3+3 macrocycle $H_3\mathbf{3}$ remained unreacted, as indicated by $^1$H NMR spectrum of the crude reaction mixture. This result corresponds to the cleavage and rearrangement of the macrocylic Schiff base, similarly as it was

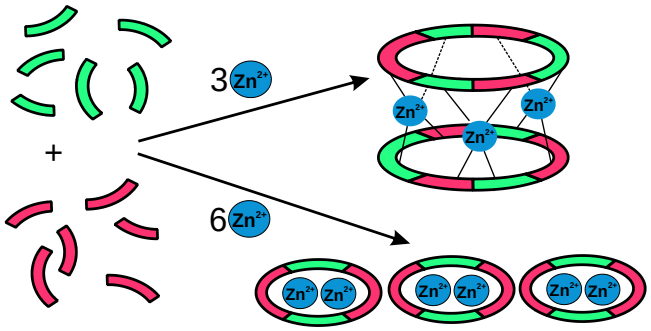


**Scheme 2**. The influence of the amount of Zn(II) template on the size of the macrocycle formed in the reaction of *1,2-trans*-diaminocyclohexane (green) and 4-*tert*-butyl-2,6-diformylphenol (red).

observed previously for other 3+3 Schiff base macrocycles.[17] It should be mentioned, however, that the $[Zn_3\mathbf{L}_2]$ (L = **1** – **4**) complexes once formed are relatively stable. For instance, heating the solutions of these cage complexes in $CDCl_3$ at 328 K for 10 days results in ca. 5 % decomposition only.

To further investigate the inertness of the $[Zn_3\mathbf{L}_2]$ complexes we measured the ROESY spectrum of a mixture of $[Zn_3\mathbf{4}_2]$, $[Zn_3\mathbf{2}_2]$ and $H_3\mathbf{4}$ (Figure S4). This spectrum does not show

exchange-type correlations between the signals of the complexed and free macrocycle, hence the dissociation of the cage complex is slow on the time scale of the NMR experiment. Moreover, this spectrum indicates different rigidity of the free and complexed macrocycles despite their very similar conformations. In the case of free $H_3$**4** clear exchange-type correlations of the two different imine signals or the two different aromatic signals can be observed (Figure S4). The presence of pairs of aromatic and azomethine signals are in accord with the *s-trans* conformation of the bis-imine fragment and the observed exchange-type correlation signals confirm the correlated bond rotation around the macrocycle.[18] Analogous correlations are not observed for the pairs of signals of [$Zn_3$**4**$_2$] indicating more rigid nature. This difference can be for instance explained by correlated bond rotation of the free macrocycle accompanied by inside-out rearrangement (Figure S4); this mechanism would not operate for [$Zn_3$**4**$_2$] because the cone conformation of the Schiff base macrocycle is frozen by cage formation.

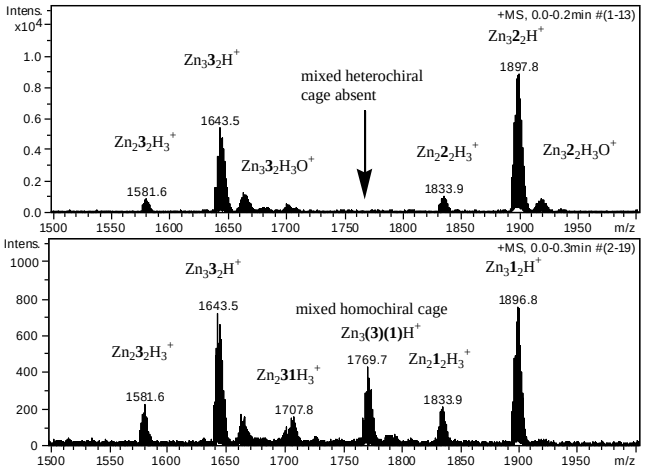


**Figure 1**. ESI MS spectra of the mixture of trinuclear complexes obtained using two different macrocycles of the opposite chirality (top) and two different macrocycles of the same chirality (bottom).

The enantiopure nature of the newly synthesized complexes is reflected in their mirror-like CD spectra (Figure S5). The crystal structures of the [$Zn_3L_2$] complexes (*vide infra*) indicate quite close contacts of the two macrocyclic units based on shape complementarity. In order to verify whether chirality plays a role in this complementarity, we have reacted 3 equivalents of Zn(II) acetate with a pseudo-racemic mixture consisting of 1 equivalent of $H_3$**2** and 1 equivalent of $H_3$**3**. The ESI mass spectrum of the resulting mixture of products indicated the trinuclear complex [$Zn_3$**3**$_2$] of the macrocycle with methyl substituents and the trinuclear complex [$Zn_3$**2**$_2$] of the macrocycle with the *tert*-butyl substituents, while the mixed trinuclear complex containing both types of macrocycles was not observed (Fig. 1). In contrast, a similar synthesis with the mixture of 1 equivalent of $H_3$**3** and 1 equivalent of $H_3$**1**, i.e. macrocycles of the same chirality, resulted in a formation of the additional mixed trinuclear complex [$Zn_3$(**1**)(**3**)] containing one macrocycle with methyl substituents and one macrocycle with tert-butyl substituents. These results clearly indicate that the trinuclear Zn(II) complex can be formed only if the two macrocyclic units are of the same chirality, which corresponds to enantiomeric self-recognition of macrocyclic ligands. Similar enantiomeric self-recognition of macrocylic units has been previously observed in the case of dinuclear lanthanide(III) complexes.[19]

The mixed homochiral complex [$Zn_3$(**1**)(**3**)] can be also observed in the $^1$H NMR spectrum, although in this case the similarity of the structures of the complexes makes the distinction of the respective signals difficult because one macrocyclic unit hardly senses the substituents on the other macrocyclic unit in the trinuclear complex. Thus most of the signals are overlapped, with the exception of the aromatic signals, where very small variations of the signals e.g. of macrocycle **3** in the [$Zn_3$**3**$_2$] and [$Zn_3$(**1**)(**3**)] complex is observed (Figure S6).

## X-ray crystal structures of the [$Zn_3L_2$] complexes

The molecular structure of the [$Zn_3$**4**$_2$] complex shows three Zn(II) ions sandwiched in between two deprotonated macrocycles **4**$^{3-}$ (Figures 2, 3). The macrocycles adopt a cone conformation with the phenolic oxygen atoms of both macrocycles pointing towards the top of the cone and at the same time pointing to the metal ions. The two macrocyclic ligands are rotated by 60 degrees with respect to each other in such a way that the diaminocyclohexane fragments of one macrocycle are situated approximately above the phenolic fragments of the other macrocycle and the whole complex is of approximate $C_3$ symmetry. This arrangement in combination with a cone conformation and close contacts between the two macrocycles results in meshing of the cyclohexane rings of the two ligands, as indicated by spacefill representation (Figure S7). The two macrocyclic units are held together by the Zn(II) ions. The Zn(II) ions are of highly distorted tetrahedral geometry with the ligand-metal-ligand angles ranging from 98$^o$ to 107$^o$ . Each Zn(II) ion is coordinated by neighbouring phenoxide oxygen atom and imine nitrogen atom of one macrocyclic unit and a similar pair of atoms from the other macrocyclic unit. In this way six of the imine nitrogen atoms of the two ligands are coordinated and point to the centre, while the other six imine nitrogen atoms are not coordinated and point outwards. This arrangement of nitrogen atoms is related to the *s-trans* arrangement of the imine bonds connected to a given aromatic ring in agreement with the $^1$H NMR spectra. Similar conformation of imine bonds was observed in the free macrocycle $H_3$**1**[20,21] or $H_3$**3**[22]. The overall shape of this trinuclear complex is similar to that of the previously reported crystal forms of [$Zn_3$**1**$_2$] grown from methanol or chloroform[8] as well as the new crystal forms of [$Zn_3$**1**$_2$], grown from toluene or from the ethanol/dichloromethane mixture, reported here (Figure 3). This shape correspond to a barrel, whose walls are built up by the macrocyclic ligands and Zn(II) ions. There are however some slight variation in the shape of this barrel. In the case of [$Zn_3$**4**$_2$] and the forms of [$Zn_3$**1**$_2$] grown from chloroform or ethanol/dichloromethane mixture the structure is somewhat more opened because the aromatic rings are arranged in a cone fashion. In the case of crystal forms of [$Zn_3$**1**$_2$] grown from methanol or toluene these rings are arranged in a more cylindrical fashion which makes the “windows” of the cage narrower. The structure in the case of [$Zn_3$**4**$_2$] is also more open because of the less bulky methyl substituents (Figure 3).

The most striking feature of these trinuclear complexes is a kind of void present in these complexes thus making them container-like molecules. The inner cavity is large enough to accommodate small guest molecules such as solvent or gas molecules. Although the two crystal structures presented here and the two structures presented previously[8] show very similar molecular structures, the packing mode is in each case different. The molecules of the complex [$Zn_3$**1**$_2$] crystallized from methanol or chloroform are positioned in the crystal lattice on top of each other forming slanted layers. In this way, narrow channels are formed along the aligned barrel-shaped complexes as well as in between complex molecules (Figure 4). In contrast, the form of this complex grown from toluene corresponds to a more compact packing and the individual barrels do not line up to form channels (Figure 4). Yet another packing is observed in the case of [$Zn_3$**4**$_2$] where individual barrels do not line up, but channels are formed in between complexed molecules (Figure 5).

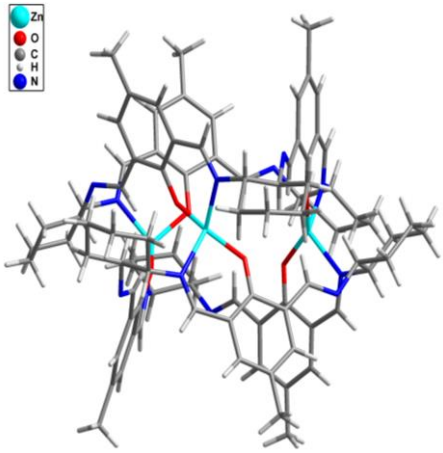


**Figure 2**. Side view of the [$Zn_3$**4**$_2$] complex (crystal form grown from methanol/chloroform solution, solvent molecules omitted).

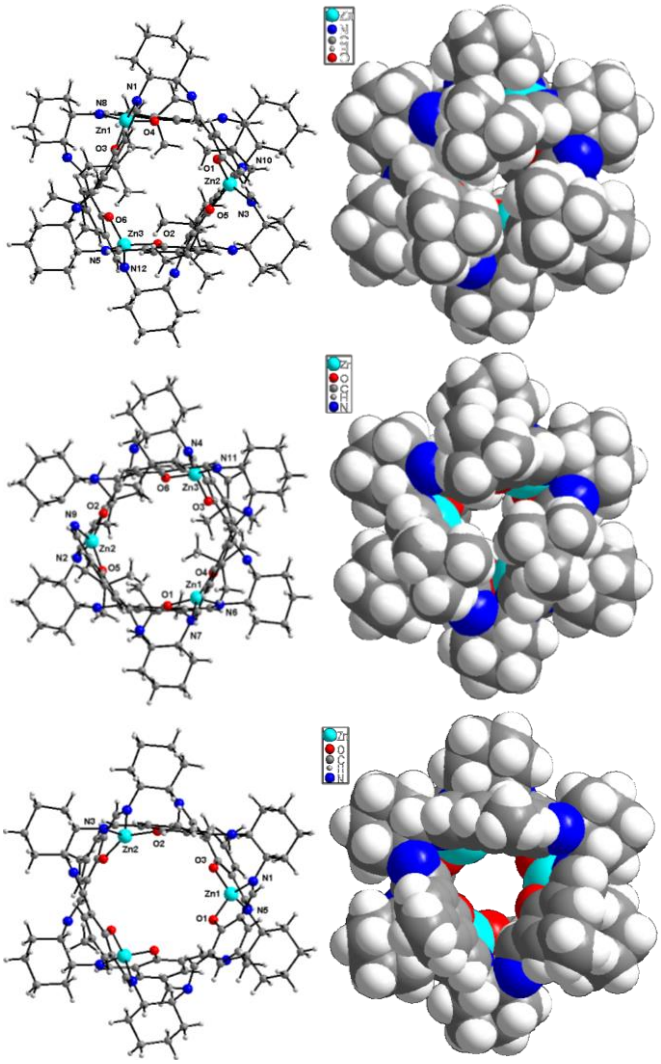

**Figure 3**. Comparison of molecular structures (top views) of [$Zn_3$**1**$_2$] form grown from toluene (top), [$Zn_3$**1**$_2$] form grown from ethanol/dichloromethane (middle) and [$Zn_3$**4**$_2$] (bottom).

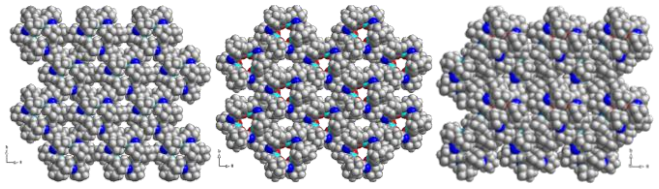

**Figure 4.** Packing of crystal forms of [$Zn_3$**1**$_2$] grown from methanol (left), chloroform (middle) and toluene (right) viewed along the c axis direction (solvent molecules omitted).

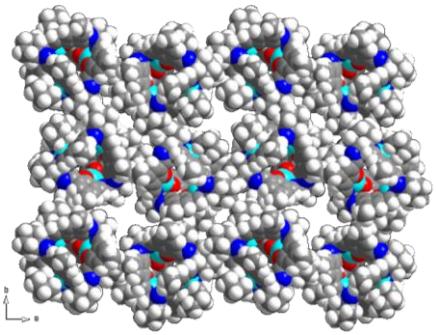

**Figure 5**. Packing of crystal of [$Zn_3$**4**$_2$] viewed along the *b* axis direction (solvent molecules omitted).

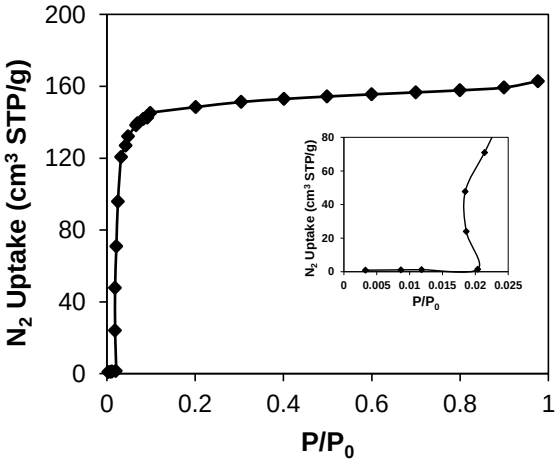


**Figure 6.** $N_2$ adsorption isotherm at 77 K in [$Zn_3$**1**$_2$]$_{act}$. Inset shows the low pressure detail of the adsorption isotherm.

## Gas adsorption properties of [$Zn_3$**1**$_2$] and [$Zn_3$**4**$_2$]

The crystal structures of [$Zn_3$**1**$_2$] and [$Zn_3$**4**$_2$] indicate their intrinsic porous nature and suggest the possibility of gas adsorption. We found that single crystals of [$Zn_3$**1**$_2$] and [$Zn_3$**4**$_2$] lose solvent rapidly when handled in air, and the framework underwent a structural transformation upon the removal of the solvent molecules in the pores, which was indicated by the shift of the peaks and the change of their intensity in the PXRD patterns (Figure S8-S9). Such structural transformation caused by desolvation process could not be proved by the single-crystal X-ray diffraction data due to the weak quality of crystals. To acquire complete solvent-free framework, as-synthesized samples of [$Zn_3$**1**$_2$] and [$Zn_3$**4**$_2$] were evacuated at ambient temperature for 24 h, yielding samples [$Zn_3$**1**$_2$]$_{act}$ and [$Zn_3$**4**$_2$]$_{act}$ that have no guest within frameworks as confirmed by $^1$H NMR and TGA analysis (Figure S10-S11). The permanent porosity of the solvent-free structures of [$Zn_3$**1**$_2$]$_{act}$ and [$Zn_3$**4**$_2$]$_{act}$ were further verified by gas adsorption experiments using $N_2$, Ar, $H_2$ and $CO_2$.

At 77 K, the $N_2$ adsorption isotherms of the [$Zn_3$**1**$_2$]$_{act}$ measured up to 1 atm displayed a particular step in the adsorption (Figures 6, S15). This isotherm showed very little $N_2$ adsorption at low pressure, followed by an abrupt increase at a gate-opening pressure[23,24] of ca. 0.02 atm, and a maximum uptake of 160 $cm^3g^{-1}$. The Brunauer-Emmett-Teller (BET) area and the total pore volume for [$Zn_3$**1**$_2$]$_{act}$ calculated from the $N_2$ adsorption isotherm are 610 $m^2g^{-1}$ and 0.24 $cm^3g^{-1}$, respectively. Such adsorption behaviours suggest the framework flexibility of the [$Zn_3$**1**$_2$] that appeared to be at a "gate closed" form after the removal of the guest molecules and underwent a structural transformation back to the "gate opened" form above the gate opening pressure. Similar behaviour has also been observed for adsorption experiment with Ar at 87 K (Figure S12). The abnormal deviations from the monotonous behaviour observed in Figures 6 and S12, are indeed also related to a gate-pressure effect. When the structure opens, it allows a very high uptake, decreasing the equilibrium pressure and resulting in a kind of "going back" section at the beginning of the plot. Similar artefacts have been reported previously for microporous inorganic-organic coordination polymers exhibiting gate-pressure effect.[24] Noteworthy, the observed pressure gating behaviour for [$Zn_3$**1**$_2$]$_{act}$ has not been reported before for any NPMs.

We further investigated the crystal structure and adsorption properties of [$Zn_3$**1**$_2$] using molecular simulation. First, we prepared three different models for the material by: i) removing the solvent molecules of the crystalline structure without modifying the position of the atoms, [$Zn_3$**1**$_2$]$_{act}$(empty); ii) performing a geometry optimization and energy minimization of the structure, modifying all the atomic positions without changing the unit cell parameters, [$Zn_3$**1**$_2$]$_{act}$(*);[25] and iii) performing the geometry optimization allowing changes in the unit cell, [$Zn_3$**1**$_2$]$_{act}$(+). Second, we predicted the gas adsorption isotherms on these three rigid models by using grand canonical Monte Carlo (GCMC) simulations. Although GCMC simulations will not distinguish between open and closed porosity, it is a broadly used technique to characterize porous materials.[26] Figure S19 shows the simulated isotherms. The Type I isotherms do not show any gate-opening effects given the rigid character of the simulations. However, the maximum adsorption capacities decrease in the order: [$Zn_3$**1**$_2$]$_{act}$(empty) > [$Zn_3$**1**$_2$]$_{act}$(*) > [$Zn_3$**1**$_2$]$_{act}$(+), i.e. when we allowed the optimization of the structure after evacuation of solvent molecules. This would confirm the existence of small flexibility in the structure that reduces the pore volume when removing guest molecules. Comparing with the experimental $N_2$ isotherm with the gate effect and given the simulated structural models, the porosity would be too narrow to allow $N_2$ adsorption at 77 K initially, so additional $N_2$ molecules and pressure are needed to open the porosity and to be absorbed in the structure.

Gas adsorption of $H_2$ at 77 K for [$Zn_3$**1**$_2$]$_{act}$ showed a Type I isotherm without any gate-pressure opening (Figure S13). The adsorbed amount of $H_2$ at 1 atm is 71 $cm^3g^{-1}$ (0.63 wt%). It can be rationalized that the narrow porosity of [$Zn_3$**1**$_2$]$_{act}$ is broad enough for $H_2$ to diffuse through the network due to the small kinetic radii (1.42 Å).[27] Figure S14 shows the $CO_2$ adsorption isotherms in [$Zn_3$**1**$_2$]$_{act}$ at 273 K. It shows a Type I isotherm with a total uptake of 7 wt % (36 $cm^3g^{-1}$ STP) at 1 bar.

GCMC adsorption isotherms for $H_2$ using the different structural models of [$Zn_3$**1**$_2$]$_{act}$ at 77 K, showed uptakes between ca. 250 and 120 $cm^3g^{-1}$ STP at 1 atm. The highest uptake corresponds to [$Zn_3$**1**$_2$]$_{act}$(empty), with the highest pore volume, whereas [$Zn_3$**1**$_2$]$_{act}$(*) and [$Zn_3$**1**$_2$]$_{act}$(+) give similar values. In a similar way, GCMC adsorption isotherms for $CO_2$ at 273 K give

uptakes between ca. 160 and 62 $cm^3g^{-1}$ (STP). These large differences between gas uptakes when allowing structural changes suggest once more the importance of taking into account flexibility in these materials.

In contrast to $[Zn_3\mathbf{1}_2]_{act}$, the $N_2$ adsorption isotherm at 77 K for $[Zn_3\mathbf{4}_2]_{act}$ revealed no significant uptake (Figure S15). This result is inconsistent with the GCMC isotherms on optimized materials (Figure S20), which again revealed Type I adsorption isotherms. Similarly, the $H_2$ (77 K) and $CO_2$ (273 K) adsorption isotherms revealed no significant uptake up to 1 atm of pressure (Figure S16-S17). This different behavior strongly suggests that $[Zn_3\mathbf{4}_2]_{act}$ shrinks either to a closed-porosity or nonporous form through the guest removal treatment. GCMC for isotherms for $N_2$, $H_2$, and $CO_2$ at 77 K and 273 K, respectively, show once more large variations in gas uptakes. These changes go up to an 85 % reduction for $N_2$ at 77 K.

### Comparison of the structures of the hydrogen-bonded dimers of the free macrocycle $H_3\mathbf{1}$ with the trinuclear Zn(II) complex $[Zn_3\mathbf{1}_2]$ and the gas adsorption properties of the free 3+3 macrocycles.

The molecular structure of the 3+3 macrocycle $H_3\mathbf{1}$,[20, 21] bearing tert-butyl substituents is similar to that of the 3+3 Schiff base $H_3\mathbf{3}$,[22] bearing methyl substituents. There are, however, striking differences in the packing of $H_3\mathbf{1}$ macrocycle crystallized from acetonitrile[20,21] and $H_3\mathbf{3}$ macrocycle crystallized form DMF[22]. While the latter forms pairs where one macrocycle act as a host for the aromatic fragment of the other macrocycle, the former macrocycle forms pairs held by hydrogen bonds. The hydrogen bonded dimers of $H_3\mathbf{1}$ form a cavity, whose shape and size is almost identical to that formed by the two macrocyclic units in the $[Zn_3\mathbf{1}_2]$ trinuclear complex (Fig. 7). The crystal structure of the $H_3$1 macrocycle crystallized from acetonitrile exhibit also a very interesting packing mode indicating the presence of two type of channels. One type of channels is formed by the joined interiors of the aligned barrel-shaped hydrogen bonded dimers. In addition, much larger channels are formed in between the macrocyclic units (Fig. 8), corresponding to an extended quasi-honeycomb network with 1D open tubular channels.

This type of crystal structure of the free ligand indicates the possibility of sorption of gas molecules. Unfortunately, the amount of crystals $H_3\mathbf{1}$ obtained from acetonitrile by slow evaporation was not sufficient to perform the gas sorption studies. Instead, we have studied the amorphous/microcrystalline form of this macrocycle precipitated from the same solvent directly in the synthesis process.

Nitrogen adsorption was measured for the activated sample of $H_3\mathbf{1}$ at 77 K. Similarly to $[Zn_3\mathbf{1}_2]_{act}$, the adsorption/desorption behaviour in $H_3\mathbf{1}$ also provides evidence of framework flexibility. As shown in Figure 9, a large step in the adsorption isotherm occurs near $P/P_o$ = 0.5, and a large hysteresis loop develops on the desorption branch. In terms of quantities adsorbed, $H_3\mathbf{1}$ adsorbs slightly more $H_2$ (75 $cm^3g^{-1}$ STP, 0.66 wt. % at 77.3 K, 1 atm; (Figure S18) than the $[Zn_3\mathbf{1}_2]_{act}$. Again, GCMC simulations on the activated sample show the existence of open porosity in the material (Figure S21). Surely, the removal of solvent molecules causes a change in the structure that impedes the $N_2$ molecules to be adsorbed at 77 K until reaching the gate pressure.

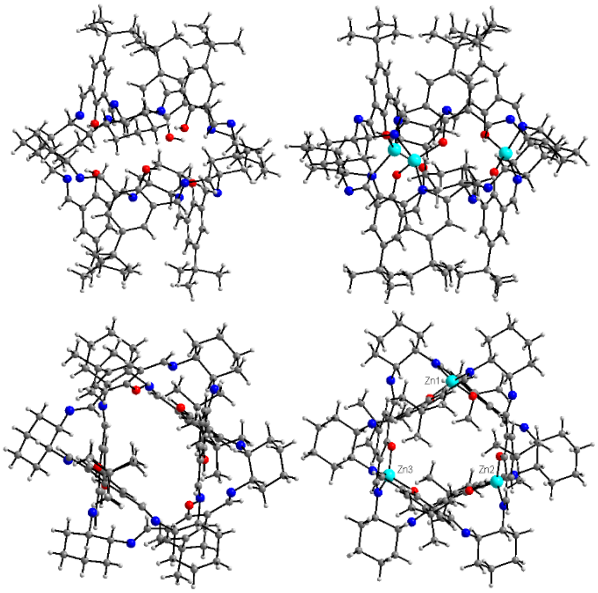


**Figure 7**. Comparison of the side and top views of the hydrogen-bonded dimer of free macrocycle $H_3\mathbf{1}$ (left) with the trinuclear complex $[Zn_3\mathbf{1}_2]$ (right)

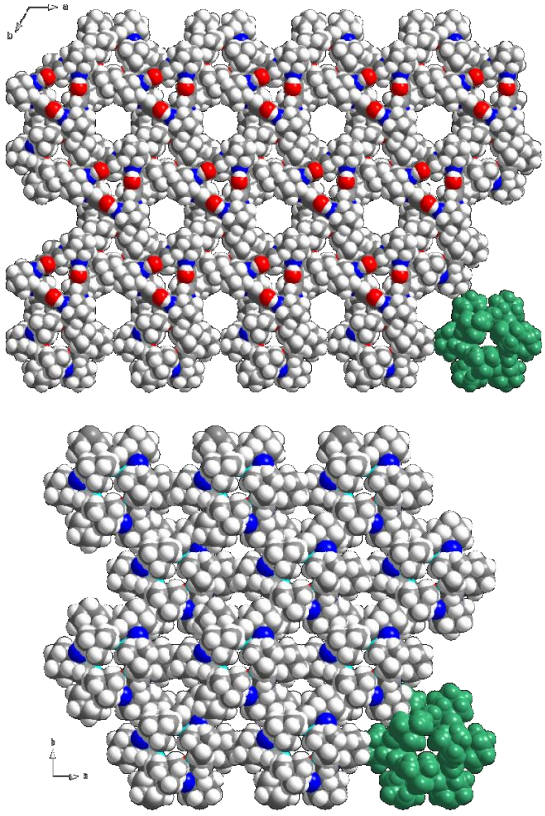

**Figure 8**. Comparison of the packing of crystals of $H_3\mathbf{1}$ grown form acetonitrile (top) with that of crystal of $[Zn_3\mathbf{1}_2]$ grown from methanol (bottom), solvent molecules omitted, a single macrocyclic dimeric $(H_3\mathbf{1})_2$ unit or $[Zn_3\mathbf{1}_2]$ molecule indicated in green.

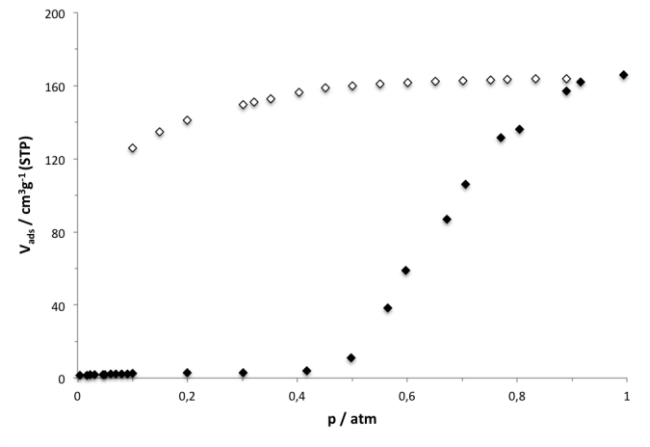


**Figure 9.** $N_2$ adsorption-desorption isotherms at 77 K for $H_3$**1**.

## Binding of chiral alcohols

The chiral nature of the studied enantiopure zinc cages and the binding of small solvent and gas molecules demonstrated above indicate the possibility of enantioselective binding of small chiral guests. As the object of preliminary investigation of such interactions we have chosen the binding of selected chiral alcohols by [$Zn_3$**1**$_2$] and [$Zn_3$**2**$_2$]. In particular the X-ray crystal structure of the crystalline form of [$Zn_3$**1**$_2$] obtained by slow evaporation of the mixture of benzene and racemic 2-butanol confirms selective binding of the enantiomers of this chiral alcohol. In this form of the [$Zn_3$**1**$_2$] cage with all-*R* chirality at the cyclohexane carbon atoms the interior is occupied by the *S*-enantiomer of sec-butanol (Figures 10, S21). In the [$Zn_3$**1**$_2$(*S*-$CH_3CH(OH)CH_2CH_3$)] complex the alcohol molecule is held by week coordination bond. One of the zinc(II) ions is five-coordinate and is bound to the oxygen atom of 2-butanol, while the other two zinc(II) ions remain four-coordinate (Figures 10, S21). Despite this, the overall shape of the cage is little changed in comparison with the native forms crystallized from chloroform, methanol or toluene. The main difference is the expansion of the phenolate oxygen – zinc – phenolate oxygen angle to the value of 155.6(2)$^o$ for the five-coordinate Zn(II) in comparison with the values of 128.2(2)$^o$ and 131.3(2)$^o$ observed for the two four coordinate Zn(II) ions. This expansion results from the fact that the available site for coordination of additional ligand in the interior of the cage is in between the phenolate oxygen atoms. However the cage is rather stiff and the flexibility of the coordination sphere around Zn(II) atoms is for this reason limited. As a consequence, the binding of additional alcohol molecule results in unfavorable small angles formed by alcohol oxygen – zinc – phenolate oxygen atoms, equal to 81.7(2)$^o$ and 79.3(2)$^o$, as well as in formation of highly distorted coordination sphere around five-coordinate zinc(II) ion, which is neither square pyramidal nor trigonal bipyramidal. This irregular geometry is also reflected by the value of the index of trigonality[28] $\tau$ equal to 0.405 ($\tau = (\beta - \alpha)/60^o$, where $\alpha$ and $\beta$ are the two largest angles in the coordination sphere around the penta-coordinate Zn(II)). The limit values of $\tau$ = 0 corresponds to an ideal square-pyramid ($\alpha = \beta \sim 180^o$) and $\tau$ = 1 to an ideal trigonal-bipyramid ($\alpha = 120^o$ and $\beta = 180^o$). The bond formed by the zinc(II) ion and alcohol hydroxyl oxygen is relatively long and is equal to 2.252(6) Å, indicating relatively weak interaction.

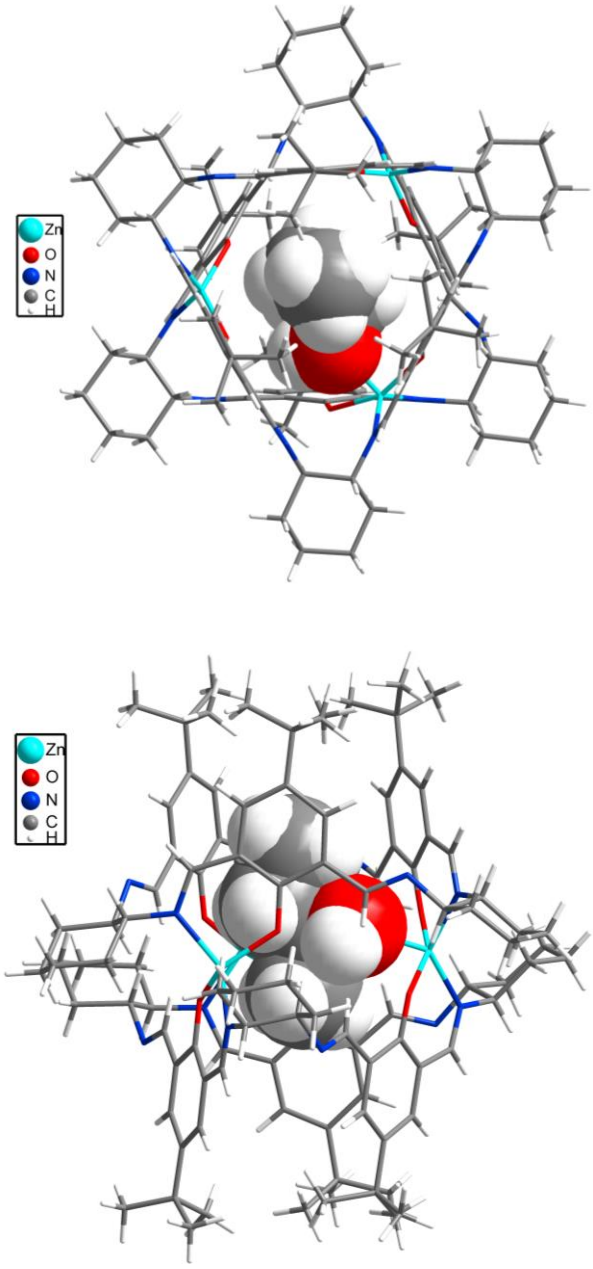


**Figure 10**. Top and side view of the [$Zn_3$**1**$_2$(*S*-$CH_3CHOHCH_2CH_3$)] cage with the coordinated (*S*)-2-butanol molecule in spacefill representation.

The molecules of [$Zn_3$**1**$_2$] in this crystalline form containing (S)-*2*-butanol align themselves on top of each other to form channels running in two directions – one along the crystallographic *a* axis and the other along the *b* axis. The crystal contains additional sec-butanol molecules that fill the space in between the cage molecules, some of them highly disordered. Thus apart from one molecule of (*S*)-2-butanol bund in the center of the zinc cage there are additional three refined molecules of this alcohol, which also correspond to the *S*-enantiomer (Figure S22). The amount of obtained [$Zn_3$**1**$_2$(*S*-$CH_3CH(OH)CH_2CH_3$)] crystals was too small to determine the ee (enantiomeric excess)

value On the other hand, the ee values obtained for the bulk samples obtained after the contact of the dried [$Zn_3$**1**$_2$] with its saturated solution in racemic 2-butanol were so far disappointingly low (13%). It seems that the different packing of the various forms of [$Zn_3$**1**$_2$], in combination with the presence of many alcohol molecules in the space in between the cage molecules, strongly affects enantioselectivity.

Enantioselective binding of chiral alcohols such as 2-butanol in the solid state was previously observed for metallomacrocyles and other materials[29]. We were interested whether in our case the different interactions of the enantiomers of chiral alcohol with the chiral cage complex operate on the level of crystalline solid only, or they occur also at molecular level in solution. For this purpose the interactions of chiral alcohols with [$Zn_3$**1**$_2$] and [$Zn_3$**2**$_2$] have been studied in solution by using NMR spectroscopy. These cage compounds turned out to be NMR chiral shift agents for 2-butanol, 2-pentanol, 1,2-butanediol, 1,3-butanediol and 1,2-propanediol (Figures 11, 12, S23-27). For instance the addition of increasing amount of [$Zn_3$**1**$_2$] to the solution of 2-butanol in deuterated toluene or benzene results in gradual splitting of NMR signal of the methyl group in position 4 (Figure 11). Similar, albeit smaller splitting was observed also for the signal of methyl group in position 1 (Figure 12). This splitting most likely results from the binding of the alcohol enantiomers by [$Zn_3$**1**$_2$] and the presence of two diastereomeric forms of host-guest complex. In order to verify whether this splitting effect is really due to spectroscopic enantiodiscrimination of 2-butanol molecules, similar $^1$H NMR spectra were recorded in the presence of enantiopure (*R*)-2-butanol and non-racemic mixtures of the *R* and *S* enantiomers (Figure 12). For the pure *R* enantiomer of alcohol no splitting of the methyl signals was observed, thus confirming the different interactions of the two isomers of 2-butanol with [$Zn_3$**1**$_2$]. The

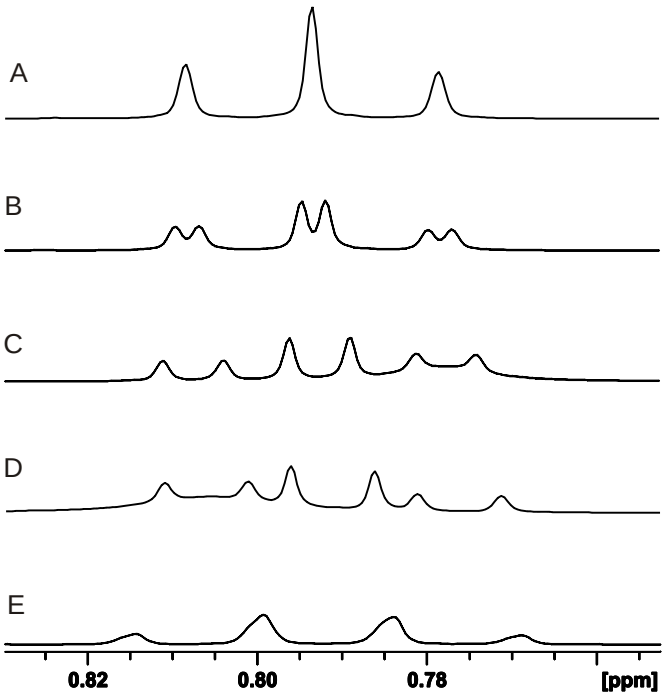


**Figure 11**. The signal of methyl group $CH_3CH(OH)CH_2CH_3$ of racemic 2-butanol (50 mM solution in toluene-$d_8$) in the presence of: 0, 0.016, 0.033, 0.069 and 0.09 equivalents of [$Zn_3$**1**$_2$] cage, traces A, B, C, D and E, respectively.

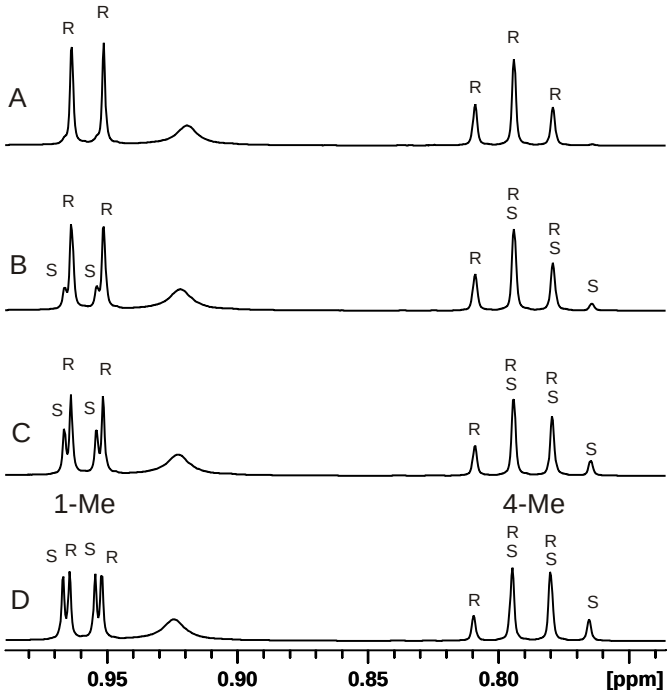


**Figure 12**. The signal of methyl groups of 2-butanol (80 mM solution in benzene) in the presence of 0.066 equivalents of [$Zn_3$**1**$_2$]: A – pure *R*-isomer of 2-butanol, B – 2:1 ratio of *R* to *S* enantiomers, , B – 5:1 ratio of *R* to *S* enantiomers, D – racemic alcohol. Labels R and L indicate the signals of the respective enantiomers of 2-butanol.

diastereomeric host-guest interaction being the origin of the observed splitting is also in accord with the correspondence of the split signal of the [$Zn_3$**1**$_2$]/racemic 2-butanol system to the sum of signals of the diastereomeric systems [$Zn_3$**1**$_2$]/(*R*)-2-butanol and [$Zn_3$**2**$_2$]/(*R*)-2-butanol (Figure S23). Similar splitting effects were observed for the solutions in deuterated chloroform, although in this latter solvent the splitting of the signals was smaller, indicating less effective competition of the alcohol molecules with the solvent molecules for the interior of the cage. The splitting of $^1$H NMR signals of methyl groups was observed also for 2-pentanol and chiral diols (Figures S24-27). In all cases studied here, the character of spectral changes observed after addition of alcohols indicate a fast chemical exchange between the alcohol molecules bound within the interior of the cage and the alcohol molecules present in bulk solution. This, together with the relatively small value of enantiomeric splitting, indicate that the binding of the alcohol molecules is not very strong. This conclusion is in agreement with the unfavorable coordination sphere of the five-coordinate Zn(II) ion observed in the crystal structure of the sec-butanol adduct.

## Conclusion

The 3+3 “calixsalene” Schiff base macrocycles $H_3$**1** – $H_3$**4** readily form 2:3 [$Zn_3$**L**$_2$] complexes in a reaction with zinc(II) acetate. In the case of [$Zn_3$**1**$_2$] the same product can be obtained in good yields directly from zinc(II) acetate, 2,6-diformyl-4-tertbutylphenol and 1,2-diaminocyclohexane precursors. In this template reaction

the size of the formed macrocyclic ligand depends upon the amount of Zn(II) template; 2+2 product is formed in a 2:2:2 reagent ratio, while 3+3 product is formed in a 1:2:2 reagent ratio. In the case of analogous template reactions of 2,6-diformyl-4-methylphenol similar tendency is observed, although the formation of 3+3 product is much less pronounced. In the $[Zn_3\mathbf{L}_2]$ complexes the two macrocycles and the rim of three Zn(II) ions form a kind of barrel with the interior occupied by solvent molecules. Strikingly similar cage-type structure is observed in the solid state for the two macrocyclic units of $H_3\mathbf{1}$ connected by hydrogen bonds. The formation of these complexes is accompanied by enantiomeric self-recognition of the chiral macrocyclic units. After removal of solvent molecules the tert-butyl derivative $[Zn_3\mathbf{1}_2]$ exhibits remarkable gas sorption properties and unique for NPMs gate-pressure effect. In contrast, the gas sorption by the methyl derivative $[Zn_3\mathbf{4}_2]$ is negligible, despite similar molecular structure of these two complexes. This difference is a result of different packing of individual cage molecules in the respective crystals. The preliminary study of binding of chiral alcohols by these trinuclear Zn(II) cages indicate enantioselective guest binding; further research along this line is currently in progress.

## Experimental Section

### Synthesis

$H_3\mathbf{1}$ ,$H_3\mathbf{2}$ , $[Zn_3\mathbf{1}_2]$ and $[Zn_3\mathbf{2}_2]$ have been obtained as described in the previous communication.[8] The macrocycle $H_3\mathbf{4}$ has been obtained in analogous way to the reported synthesis of $H_3\mathbf{3}$[30] starting from *(1S),(2S)-trans*-diaminocyclohexane.

$[Zn_3\mathbf{4}_2]\cdot 3CH_3OH$: The suspension of 154 mg of $H_3\mathbf{4}$ (0.2 mmol) in 6 mL of methanol was combined with 66 mg of $Zn(CH_3COO)_2\cdot 2H_2O$ (0.3 mmol) and the mixture was stirred at room temperature for 1 hour. The yellow suspension was filtered, washed with 1 mL of methanol and dried. Yield 60 mg, 34%. $^1$H NMR (500 MHz, CDCl3, $\delta$=7.26 ppm): $\delta$ =0.84 ppm (m), 1.15 (m), 1.27 (m), 1.58 (m), 1.67 (m), 1.82 (d, J=10.8Hz), 3.29 (m), 3.76 (m), 6.85 (d, J=2.0 Hz), 7.67 (d, J=2.0 Hz), 8.02 (s), 9.50 (s); ESI/MS: *m/z* (%): 1643.5 $[Zn_3\mathbf{3}_2H^+]$, elemental analysis calcd (%) for $C_{93}H_{114}N_{12}O_9Zn_3$: C 64.19, H 6.60, N 9.66; found: C 64.11, H 6.47, N 9.84.

$[Zn_3\mathbf{3}_2]\cdot 3CH_3OH$ has been obtained in analogous way as $[Zn_3\mathbf{4}_2]\cdot 3CH_3OH$ starting from $H_3\mathbf{3}$.

$[Zn_2\mathbf{6}(AcO)_2]\cdot H_2O$: 2,6-diformyl-4-methylphenol (100mg, 0.609 mmol) was dissolved in 25 mL of methanol and combined with solid $Zn(CH_3COO)_2\cdot 2H_2O$ (135mg, 0.609 mmol) and a solution of *(1R),(2R)-trans*-diaminocyclohexane (92mg, 0.609 mmol) in 25 mL of methanol. The mixture was refluxed for 1h, cooled down and the formed precipitate was filtered, washed with methanol and dried in vacuum. Yield 110 mg, 51%. $^1$H NMR (500 MHz, CDCl3): $\delta$=1.48 (m), 1.69 (m), 1.74 (m), 2,01 (d, J=7.3 Hz), 3,40 (s), 4,04 (s), 7,17 (s), 8,26 (s) ESI/MS: *m/z*: 671,13 [C30H34N4O2Zn2CH3COO$^+$], elemental analysis calcd (%) for $C_{34}H_{42}N_4O_7Zn_2$: C(54.48) H(5.65) N(7.47); found: C (54.44) H(5.58) N(7.24).

### Methods

The NMR spectra were measured on Bruker Avance 500 spectrometer. The positive-mode electrospray mass spectra of methanol solutions of the complexes were obtained using Bruker microOTOF-Q instrument. The CD spectra were measured on Jasco J-715 Spectropolarimeter. The elemental analyses were carried out on a Perkin-Elmer 2400 CHN elemental analyzer.

### Molecular Simulations

Structural models of the porous structures were obtained from $[Zn_3\mathbf{1}_2]$ and $[Zn_3\mathbf{4}_2]$. The lattice parameters were initially not modified ($[Zn_3\mathbf{1}_2]$: a = Å, b = Å, c = Å; $[Zn_3\mathbf{4}_2]$: a = Å, b = Å, c = Å). Thereafter, the structures were subject to geometry optimization based on molecular mechanics calculations, modifying all the atomic positions. Three models were prepared for $[Zn_3\mathbf{1}_2]$ by: i) removing the solvent molecules of the crystalline structure without modifying the position of the atoms, $[Zn_3\mathbf{1}_2]_{act}$(empty); ii) performing a geometry optimization and energy minimization of the structure, modifying all the atomic positions without changing the unit cell parameters, $[Zn_3\mathbf{1}_2]_{act}$(*); and iii) performing the geometry optimization allowing changes in the unit cell $[Zn_3\mathbf{1}_2]_{act}$(+). Three analogous structures were obtained for $[Zn_3\mathbf{4}_2]$, plus two additional ones, without and with energy minimization: $[Zn_3\mathbf{1}_2]_{act}$(UFF*) and $[Zn_3\mathbf{1}_2]_{act}$(UFF+) respectively, where the lattice parameters were obtained from indexing the experimental powder X-ray diffraction pattern of $[Zn_3\mathbf{4}_2]_{act}$. These calculations were performed with the Forcite module of Materials Studio, using an algorithm that is a cascade of the steepest descent, adjusted basis set Newton − Raphson, and quasi-Newton methods. The bonded and the short-range (van der Waals) nonbonded interactions between the atoms were modelled using the Universal Force Field (UFF). In UFF, bond stretching is described by a harmonic term, angle bending by a three-term Fourier cosine expansion, torsions and inversions by cosine-Fourier expansion terms, and the van der Waals interactions by the Lennard-Jones (LJ) potential. A cut-off distance of 12 Å was used for the LJ interactions. The long-range, electrostatic, interactions, arising from the presence of partial atomic charges, were modelled using a Coulombic term. The Ewald sum method was used to compute the electrostatic interactions. Partial atomic charges were derived from the charge equilibration method (QEq) as implemented in Forcite.

The adsorption of $N_2$, $CH_4$, $CO_2$ and $H_2$ was investigated using grand canonical Monte Carlo (GCMC) simulations, performed with the in-house multi-purpose code RASPA.[31] Quantum diffraction effects using Feynman-Hibbs corrections were used in the simulations of $H_2$.[32] We used a rigid atomistic model for all the structures, in which the framework atoms were kept fixed. Solid-fluid and fluid-fluid interactions were calculated using a Lennard-Jones (LJ) + Coulomb potential. LJ parameters for the framework atoms were taken from the Universal Force Field (UFF),[33] the $N_2$, $CH_4$ and $CO_2$ LJ parameters from the TraPPE force field,[34] and the $H_2$ LJ parameters were taken from an empirical model for $H_2$.[35] Lorentz-Berthelot mixing rules were used for all cross terms, and LJ interactions beyond 12 Å were neglected. Coulomb interactions were calculated using partial charges on the framework atoms (as described in Section S1) and $H_2$ charges taken from the Darkrim-Levesque[36] model. The Ewald sum method was used to compute the electrostatic interactions. $6\cdot 10^4$ Monte Carlo equilibration cycles were performed plus $4\cdot 10^4$ production cycles to calculate the ensemble averages. In one cycle, an average of *N* moves were performed, where *N* is the number of molecules in the system (which fluctuates in GCMC). Monte Carlo moves used with equal probability were translation, rotation, insertion, deletion, and random reinsertion of an existing molecule at a new position. To calculate the gas-phase fugacity, we used the Peng-Robinson (PR) equation of state (EOS).[37] The pore volume, used to compute excess adsorption from the simulated absolute adsorption, was obtained using a Widom particle insertion method, by probing the structure with a helium molecule at room temperature, recording a large number of random points not overlapping the van der Waals volume of the framework.[38]

### X-ray crystallography

Single crystals of $Zn_3\mathbf{4}_2$ were grown from methanol/chloroform solution(**I**, tetragonal, $P4_32_12$), the new modifications of $Zn_3\mathbf{1}_2$ crystals were grown from toluene (**II**, monoclinic, $P2_1$), ethanol/dichloromethane (**III**, trigonal, $P3_2$) or benzene/racemic 2-butanol solution (**IV**, trigonal, $P3_2$) and the crystals of $H_3\mathbf{1}$ were grown from acetonitrile solution (**V**, hexagonal, $P6_322$). X-ray single crystal data collection was performed using graphite monochromatic MoK$\alpha$ radiation on a four-circle $\kappa$ geometry KUMA KM-4 diffractometer with a two-dimensional area CCD detector at 100(2)K. The $\omega$-scan technique with $\Delta\omega$ = 1.0$^o$ for each image was used for data collection. One image was used as a standard after every 50 images for monitoring of the crystals stability and the data collection. No correction on the relative intensity variations was necessary. Data collections were made using the CrysAlis CCD program [39]. Integration, scaling of the reflections, correction for Lorentz and polarisation effects and absorption corrections were performed using the CrysAlis Red program [39]. The structures were solved by the direct methods using SHELXS-97 and refined

with anisotropic displacement parameters using SHELXL-97 program [40]. The hydrogen atoms were introduced in their geometrical positions and refined with isotropic displacement parameters. Some of the solvent molecules, i.e. toluene in the crystal **I**, methanol and water in the crystal **II**, ethanol and dichloromethane in the crystal **III,** 2-butanol in crystal **IV** were possible to be localised, and they were refined. The rest of the solvent molecules in **I-IV** and all acetonitrile solvent molecules in the crystal **V** are highly disordered. Correct modelling of the disorders was not possible and we proceeded to a "squeeze" treatment to remove the scattering contribution of these molecules, which could not to be satisfactory modelled. The final difference Fourier maps showed no peaks of chemical significance. Details of the data collection parameters, crystallographic data and final agreement parameters are collected in Table 1. Visualizations of the structures were made with the Diamond 3.0 and Mercury 3.5 programs [41,42]. CCDC 1056109, 1056110, 1056111, 1419795 and 1056112 contain the supplementary data for crystals **I**, **II**, **III, IV** and **V**. These data can be obtained free of charge from The Cambridge Crystallographic Data Centre via www.ccdc.cam.ac.uk/data request/cif.

## Acknowledgements

This work was supported by NCN grant 2011/03/B/ST5/01060. D.P. and J.L. thanks the FNP Program "Mistrz" for financial support, and D.F.-J. thanks the Royal Society for funding through a University Research Fellowship.

**Keywords:** macrocycles • zinc • cages • porosity • self-recognition

[1] a) N. B. McKeown, *J. Mater. Chem*. **2010**, 20, 10588 – 10597; b) J. Tian, P. K. Thallapally, B. P. McGrail, *CrystEngComm*, **2012**, *14*, 1909-1919.

[2] a) J. R. Holst, A. Trewin, A. I. Cooper, *Nat. Chem*. **2010**, *2*, 915 – 920; b) M. Mastalerz, *Chem. Eur. J.* **2012**, *18*, 10082–10091; c) G. Zhang, M. Mastalerz *Chem. Soc. Rev*. **2014**, *43*, 1934-1947; d) A. I. Cooper, *Angew. Chem. Int. Ed.* **2012**, *51*, 7892 – 7894; e) M. Mastalerz, *Angew. Chem. Int. Ed*. **2012**, *51*, 584 – 586; f) J. Tian, P. K. Thallapally, S. J. Dalgarno, P. B. McGrail, J. L. Atwood, *Angew. Chem. Int. Ed.* **2009**, *48*, 5492 – 5495; g) W. Yang, A. Greenaway, X. Lin, R. Matsuda, A. J. Blake, C. Wilson, W. Lewis, P. Hubberstey, S. Kitagawa, N. R. Champness,, M. Schroder, *J. Am. Chem. Soc.* **2010**, *132*, 14457-14469; h) J. Lu, C. Perez-Krap, M. Suyetin, N. H. Alsmail, Y. Yan, S.i Yang, W. Lewis, E. Bichoutskaia, C. C. Tang, A. J. Blake, R. Cao, M. Schroder, *J. Am. Chem. Soc*. **2014**, *136*, 12828-12831; i) S. Lim, H. Kim, N. Selvapalam, K.-J. Kim, S. J. Cho, G. Seo, Ki. Kim, *Angew. Chem. Int. Ed*. **2008**, *47*, 3352-3355; j) H. Kim, Y. Kim, M. Yoon, S. Lim, S. M. Park, G. Seo, K. Kim, *J. Am. Chem. Soc.* **2010**, *132*, 12200-2202.

[3] a) J. An, R. P. Fiorella, S. J. Geib, N. L. Rosi, *J. Am. Chem. Soc*., **2009**, *131*, 8401–8403; b) P. S. Nugent, V. L. Rhodus, T. Pham, K. Forrest, L. Wojtas, B. Space, M. J. Zaworotko, *J. Am. Chem. Soc*. **2013**, *135*, 10950 – 10953; c) R. Murugavel, S. Kuppuswamy, N. Gogoi, R. Boomishankar, A. Steiner, *Chem. Eur. J.* **2010**, *16*, 994 – 1009; d) I. Bassanetti, F. Mezzadri, A. Comotti, P. Sozzani, M. Gennari, G. Calestani, L. Marchio, *J. Am. Chem. Soc.* **2012**, *134*, 9142−9145; e) K. Sokołowski, W. Bury, D. Fairen-Jimenez, I. Justyniak, K. Sołtys, D. Prochowicz, S. Yang, M. Schröder, J. Lewiński, *Angew. Chem. Int. Ed.* **2013**, *52,* 13414–13418.

[4] T. Kaczorowski, I. Justyniak, T. Lipińska, J. Lipkowski, J. Lewiński, *J. Am. Chem. Soc*. **2009**, *131*, 5393 – 5395.

[5] J. Lewiński, T. Kaczorowski, D. Prochowicz, T. Lipińska, I. Justyniak, Z. Kaszkur, J. Lipkowski, *Angew. Chem. Int. Ed*. **2010**, *49*, 7035 – 7039.

[6] a) R. A. Smaldone, R. S. Forgan, H. Furukawa, J. J. Gassensmith, A. M. Z. Slawin, O. M. Yaghi, J. F. Stoddart, *Angew. Chem. Int. Ed*. **2010,** *49*, 8630 – 8634; b) Y. Wei, D. Sun, D. Yuan, Y. Liu, Y. Zhao, X. Li, S. Wang, J. Dou, X. Wang, A. Hao, *Chem. Sci*. **2012**, *3*, 2282−2287.

[7] S. Kitagawa, K. Uemura, *Chem. Soc. Rev*. **2005**, *34*, 109-119.

[8] A. Sarnicka, P. Starynowicz, J. Lisowski, *Chem. Commun*. **2012**, *48*, 2237–2239.

[9] a) C. Zhao, J. Ren, J. Gregolinski, J. Lisowski, X. Qu, *Nucleic Acids Res*. **2012**, *40*, 8186 – 8196; b) A. González-Alvarez, I. Alfonso, J. Cano, P. Díaz, V. Gotor, V. Gotor-Fernández, E. García-España, S. Garcia-Granda, H. R. Jiménez, G. Lloret, *Angew. Chem. Int. Ed*. **2009**, 48, 6055-6058; c) J. Gregoliński, P. Starynowicz, K. T. Hua, J. L. Lunkley, G. Muller, J. Lisowski, *J. Am. Chem. Soc.* **2008**, *130*, 17761–17773; d) J. Gregoliński, T. Lis, M. Cyganik, J. Lisowski, *Inorg. Chem*. **2008**, *47*, 11527-11534; e) J. Gregoliński, J. Lisowski, *Angew. Chem. Int. Ed*. **2006**, *45*, 6122-6126.

[10] a) M. J. Kobyłka, K. Ślepokura, M. Acebrón Rodicio, M. Paluch. J. Lisowski, *Inorg. Chem*. **2013**, *52*, 12893 – 12903; b) S.-Y. Lin, Y.-N. Guo, Y. Guo, L. Zhao, P. Zhang, H. Ke, J. Tang, *Chem. Commun*, **2012**, *48*, 6924-6926; c) J. Gajewy, J. Gawroński, M. Kwit, *Org. Biomol. Chem*. **2011**, *9*, 3863-3870; d) J. Gao, R. A. Zingaro, J. H. Reibenspies, A. E. Martell, *Org. Lett.* **2004**, *6*, 2453 – 2455.

[11] a) S. Tashiro, R. Kubota, M. Shionoya, *J. Am. Chem. Soc*. **2012**, *134*, 2461 – 2464; b) S. Tashiro, T. Umeki, R. Kubota, M. Shionoya, *Angew. Chem. Int. Ed.* **2014**, *53*, 8310 – 8315.

[12] a) D. A. Fowler, A. S. Rathnayake, S. Kennedy, H. Kumari, C. M. Beavers, S. J. Teat, J. L. Atwood, *J. Am. Chem. Soc*. **2013**, *135*, 12184-12187; b) S. J. Dalgarno, N. P. Power, J. L. Atwood, *Coord. Chem. Rev*. **2008**, *252*, 825-841.

[13] a) T. K. Ronson, S. Zarra, S. P. Black, J. R. Nitschke, *Chem. Commun*. **2013**, *49*, 2476-2490; b) P. D. Frischmann, M. J. MacLachlan, *Chem. Soc. Rev*. **2013**, *42*, 871-890; c) N. M. Rue, J. Sun, R. Warmuth *Isr. J. Chem*. **2011**, *51*, 743-768.

[14] a) W. Xuan, M. Zhang, Y. Liu, Z. Chen, Y. Cui, *J. Am. Chem. Soc*. **2012**, *134*, 6904-6907; b) I. A. Riddel, M. M. J. Smulders, J. K. Clegg, J. R. Nitschke, *Chem. Commun.* **2011**, *47*, 457-459; c) A. Granzhan, T. Riis-Johannessen, R. Scopelliti, K. Severin, *Angew. Chem. Int. Ed*. **2010**, *49*, 5515-5518.

[15] M. M. Safont-Sempere, G. Fernández, F. Würthner, *Chem. Rev*. **2011**, *111*, 5784-5814.

[16] Selected examples of enantiomeric self-recognition of ligands: a) M. Boiocchi, L. Fabbrizzi, *Chem. Soc. Rev*. **2014**, *43*, 1835-1847; b) H. S. Jena, *RSC Adv*. **2014**, *4*, 3028-3044; c) C. Gütz, R. Hovorka, G. Schnakenburg, A. Lützen, *Chem. Eur. J.* **2013**, *19*, 10890-10894; d) J.-C. Buffet, J. Okuda, P. L. Arnold,, *Inorg. Chem.* **2010**, *49*, 419-426; e) P. L. Arnold, J.-C. Buffet, R. Blaudeck, S. Sujecki, C. Wilson, *Chem. Eur. J*. **2009**, *15*, 8241-8250; f) P. L. Arnold, J.-C. Buffet, R. P. Blaudeck, S. Sujecki, A. J. Blake, C. Wilson, *Angew. Chem. Int. Ed*. **2008**, *47*, 6033-6036; g) M. Lama, O. Mamula, S. Kottas, L. De Cola, H. Stoeckli-Evans, S. Shova, *Inorg. Chem.* **2008**, *47*, 8000-8015; h) M. Lama, O. Mamula, G. S. Kottas, F. Rizzo, L. De Cola, A. Nakamura, R. Kuroda, H. Stoeckli-Evans, *Chem. Eur. J.* **2007**, *13*, 7358-7373; i) H.-J. Kim, D. Moon, M. S. Lah, J.-I. Hong,,*Angew. Chem. Int. Ed*. **2002**, *41*, 3174-3177; j) M. Steigelmann, Y. Nisar, F. Rominger, B. Goldfuss, *Chem. Eur. J*. **2002**, *8*, 5211-5218; k) J. Lewiński, J. Zachara, I. Justyniak, *Chem. Commun.*, **1997**, 1519-1520.

[17] a) J. Gao, J. H. Reibenspies, R. A. Zingaro, F. R. Woolley, A. E. Martell, A. Clearfield, *Inorg. Chem*. **2005,** *44*, 232; b) J.-C. Jiang, Z.-L. Chu, W. Huang, G. Wang, X.-Z. You, *Inorg. Chem*. **2010**, *49*, 5897; c) S. R. Korupoju, N. Mangayarkarasi, S. Ameerunisha, E.J. Valente, P. S. Zacharias, *J. Chem. Soc. Dalton Trans*. **2000**, 2845.

[18] a) M. Kwit, J. Gawroński, *Tetrahedron: Assymetry*, **2003**, *14*, 1303-1308; b) J. Gawroński, H. Kołbon, M. Kwit, A. Kartusiak, *J. Org. Chem*. **2000**, *65*, 5768-5773.

[19] J. Lisowski, *Inorg. Chem*. **2011**, *50*, 5567-5576.

[20] Y. Fu, Z. Xing, C. Zhu, H. Yang, W. He, C. Zhu, Y. Cheng, *Tetrahedron Lett.* **2012**, *53*, 804-807.

[21] We have independently re-determined the crystal structure of the crystals of the $H_3$**1** macrocycle grown from acetonitrile using SQUEEZE procedure and obtaining similar result to that reported in ref [20].

[22] M. Paluch, J. Lisowski, T. Lis, Dalton Trans. 2006, 381-388.

[23] D. Li, K. Kaneko, Chem. Phys. Lett. 2001, 335, 50-56;

[24] a) H. Chun, J. Seo, Inorg. Chem. 2009, 48, 9980–9982; b) H. Tanaka, S. Ohsaki, S. Hiraide, D. Yamamoto, S. Watanabe, M. T. Miyahara, J. Phys. Chem. C 2014, 118, 8445−8454.

[25] a) W. Bury, D. Fairen-Jimenez, M. B. Lalonde, R. Q. Snurr, O. K. Farha, J. T. Hupp, Chem. Mater. 2013, 25 , 739–744; b) D. Fairen-Jimenez, Y. J. Colon, O. K. Farha, Y.-S. Bae, J. T. Hupp, R. Q. Snurr, Chem. Commun., 2012, 48, 10496–10498; c) N. L. Strutt, D. Fairen-Jimenez, J. Iehl, M. B. Lalonde, R. Q. Snurr, O. K. Farha, J. T. Hupp, J. F. Stoddart, J. Am. Chem. Soc. 2012, 134, 17436–17439.

[26] a) D. Fairen-Jimenez, N. A. Seaton, T. Düren, *Langmuir*, **2010**, *26*, 14694–14699; b) D. Fairen-Jimenez, S. A. Moggach, M. T. Wharmby, P. A. Wright, S. Parsons, T. Düren, *J. Am. Chem. Soc.*, **2011**, *133*, 8900–8902; c) D. Fairen-Jimenez, R. Galvelis, A. Torrisi, A. D. Gellan, M. T. Wharmby, P. A. Wright, C. Mellot-Draznieks, Tina Düren, *Dalton Trans*. **2012**, *41*, 10752-10762.

[27] J. M. Seco, D. Fairen-Jimenez, A. J. Calahorro, L. Méndez-Liñán, M. Pérez-Mendoza, N. Casati, E. Colacioc, A. Rodríguez-Diéguez, *Chem. Commun.*, **2013**, 49, 11329-11331.

[28] A. W. Addison, T. N. Rao, J. Reedijk, J. van Rijn, G. C. Verschoor, *J. Chem. Soc., Dalton Trans*., **1984**, 1349-1356.

[29] See for instance: a) G. Li, W. Yu, J. Ni, T. Liu, Y. Liu, E. Sheng, Y. Cui, *Angew. Chem. Int. Ed*. **2008**, *47*, 1245 –1249; b) G. Li, W. Yu, Y. Cui, *J. Am. Chem. Soc.* **2008**, 130, 4582-4583; c) Y. Li, D. Yu, Z. Dai, J. Zhang, Y. Shao, N. Tang, Ji. Wu, *Dalton Trans*., **2015**, *44*, 5692–5702; d) P. Li, Y. He, J. Guang, L. Weng, J. C.-G. Zhao, S. Xiang, B. Chen, *J. Am. Chem. Soc.* **2014**, *136*, 547−549.

[30] S. R. Korupoju, P. S. Zacharias, *Chem. Commun.* **1998**, 1267-1269.

[31] a) D. Dubbeldam, S. Calero, D. E. Ellis, R. Q. Snurr (2015): RASPA: molecular simulation software for adsorption and diffusion in flexible nanoporous materials, Molecular Simulation; b) D. Frenkel, B. Smit, *Understanding Molecular Simulations: From Algorithms to Applications*, 2nd ed. edn., Academic Press, San Diego, **2002**.

[32] a) A. Rossin, D. Fairen-Jimenez, T. Düren, G. Giambastiani, M. Peruzzini, J. G. Vitillo, *Langmuir*, **2011**, 27, 10124–10131; b) D. Fairen-Jimenez, Y. J. Colón, O. K. Farha, Y.-S. Bae, J. T. Hupp, R. Q. Snurr, *Chem. Commun*. **2012**, *48*, 10496-10498; c) A. K. Rappé, C. J. Casewit, K. S. Colwell, W. A. G. III and W. M. Skiff, *J. Am. Chem. Soc.*, **1992**, *114*, 10024-10035.

[33] A. K. Rappé, C. J. Casewit, K. S. Colwell, W. A. G. III and W. M. Skiff, *J. Am. Chem. Soc.*, **1992**, *114*, 10024-10035.

[34] a) J. J. Potoff, J. I. Siepmann, *AIChE J*., **2001**, 47, 1676–1682; b) M. G. Martin, J. I. Siepmann, *J. Phys. Chem. B*, **1998**, 102, 2569–2577.

[35] A. Michels, W. Degraaff, C. A. Tenseldam, *Physica*, **1960**, *26*, 393.

[36] F. Darkrim, D. Levesque, J. Chem. Phys. **1998**, *109*, 4981-4984

[37] Reid, R. C. Prausnitz, J. M. Poling, B. E. *The Properties of Gases and Liquids*, 4th ed.; McGraw-Hill: New York, **1987**.

[38] A. Leach, *Molecular modelling : principles and applications*, Pearson Prentice Hall, **2001**.

[39] CrysAlis CCD and CrysAlis Red, Version 171.33.48, Oxford Diffraction Poland, Wrocław, Poland (2009).

[40] G. M. Sheldrick, *SHELXS97*, *SHELXL97*, Programs for Crystal Structures Solution and Refinement, University of Göttingen, Göttingen, Germany, 1997.

[41] K. Brandenburg, H. Putz, DIAMOND Version 3.0, Crystal Impact GbR, Bonn, Germany, (2006).

[42] MERCURY, Ver. 3.5.1, Programme for Crystal Structure Visualisation and Exploration, CCDC Cambridge University 2014.

Received: ((will be filled in by the editorial staff))
Revised: ((will be filled in by the editorial staff))
Published online: ((will be filled in by the editorial staff))

Table 1. Crystal data and final refinement parameters for I-IV crystals.

| Crystal | **I** | **II** | **III** | **IV** | **V** |
|---|---|---|---|---|---|
| Compound | $Zn_3\mathbf{4}_2$ | $Zn_3\mathbf{1}_2$ | $Zn_3\mathbf{1}_2$ | $[Zn_3\mathbf{1}_2$(*S*-butanol-2] | $H_3\mathbf{1}$ |
| Crystallization medium | chloroform/methanol | toluene | ethanol/dichloromethane | benzene/2-butanol | acetonitrile |
| Formula | $C_{97}H_{136}N_{12}O_{17.5}Zn_3$ | $C_{129}H_{174}N_{12}O_9Zn_3$ | $C_{108}H_{138}N_{12}O_6Zn_3$ | $C_{124}H_{178}N_{12}O_{10}Zn_3$ | $C_{54}H_{72}N_6O_3$ |
| Mol. weight | 1946.29 | 2232.90 | 1896.41 | 2192.89 | 853.18 |
| Crystal System | tetragonal | monoclinic | trigonal | trigonal | hexagonal |
| Space Group | $P4_32_12$ | $P2_1$ | $P3_2$ | $P3_2$ | $P6_322$ |
| *a,* [Å] | 30.7617(8) | 17.1927(5) | 17.5761(3) | 18.0892(3) | 18.6583(7) |
| *b,* [Å] | 30.7617(8) | 20.4415(6) | 17.5761(3) | 18.0892(3) | 18.6583(7) |
| *c,* [Å] | 11.0198940 | 18.9242(6) | 38.2192(10) | 38.3863(10) | 22.1979(10) |
| α,β,γ [°] | 90/90/90 | 90/101.57(1)/90 | 90/90/120 | 90/90/120 | 90/90/120 |
| V [Å$^3$] | 10427.8(5) | 6515.7(3) | 10224.9(4) | 10877.9(4) | 6692.5(5) |
| T [K] | 100(2) | 100(2) | 100(2) | 100(2) | 100(2) |
| λ, Mo$K_\alpha$ | 0.71073 | 0.71073 | 0.71073 | 0.71073 | 0.71073 |
| Crystal Size | 0.33×0.31×0.25 | 0.28×0.23×0.21 | 0.38×0.32×0.24 | 0.32×0.27×0.21 | 0.37×0.32×0.24 |
| μ, [mm$^{-1}$] | 0.751 | 0.605 | 0.567 | 0.543 | 0.053 |
| Θ range [°] | 2.71 ÷ 28.91 | 2.89 ÷ 33.66 | 2.82 ÷ 28.50 | 2.81 ÷ 28.8 | 2.85 ÷ 30.0 |
| Tmin./Tmax. | 0.7916/08411 | 0.8554/0.8914 | 0.7620/0.8393 | 0.8565/0.9062 | 0.9833/0.9894 |
| Refls collceted | 38003 | 70466 | 86371 | 79126 | 83536 |
| Independent refls | 12359 | 40183 | 36528 | 34668 | 10888 |
| Observed refls [I>2σ(I)] | 9155 | 21233 | 20214 | 17415 | 5680 |
| $R_{int}$ | 0.0639 | 0.0739 | 0.0604 | 0.0704 | 0.0712 |
| L. S. parameters | 603 | 1387 | 1154 | 1371 | 194 |
| R1 [I>2σ(I)] | 0.0763 | 0.0637 | 0.0646 | 0.0868 | 0.0684 |
| wR2 (all refls) | 0.1743 | 0.1217 | 0.1407 | 0.1757 | 0.1289 |
| S | 0.994 | 1.002 | 0.984 | 0.938 | 1.001 |
| Flack parameter | 0.057(14) | 0.010(6) | 0.027(8) | 0.027(11) | -0.01(2) |
| Largest diff peak and hole [eÅ$^{-3}$] | 0.782 and -0.471 | 1.083 and -0.580 | 0.347 and -0.209 | 1.275 and -0.704 | 0.226 and -0.126 |

R1=Σ||$F_o$|–|$F_c$||/Σ|$F_o$|; wR2={Σ [$w(F_o^2–F_c^2)^2$]/Σ$wF_o^4$}$^{½}$; $w^{-1}$=1/[$\sigma^2(F_o^2)$ + $(aP)^2$ +$bP$ ] where $a$=0.09 and $b$=4.9074 for **I**, $a$=0.0295 and $b$=0 for **II**, $a$=0.0430 and $b$=0 for **III**, $a$=0.010 and $b$=0.0 for **IV** and $a$=0.0390 and $b$=0 for **V** and $P$ = ($F_o^2$ + 2$F_c^2$)/3.

DOI: 10.1002/chem.201xxxxxx


**Entry for the Table of Contents**

## FULL PAPER

Two deprotonated macrocyclic 3+3 triphenolic macrocycles bind three zinc(II) cations to form a barrel-shaped $[Zn_3L_2]$ complexes. The formation of these complexes is accompanied by enantiomeric self-recognition of the macrocyclic units. The cage-like structure of the $[Zn_3L_2]$ complexes leads to binding of chiral alcohol molecules and to a porous nature reflected in remarkable gas adsorption properties.

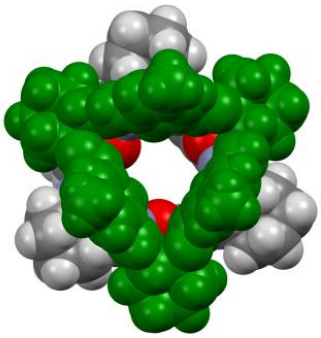

**chiral Zn(II) cages**

*Jan Janczak, Daniel Prochowicz, Janusz Lewiński, David Fairen-Jimenez, Tomasz Bereta and Jerzy Lisowski**

■■ – ■■

**Trinuclear cage-like Zn(II) macrocyclic complexes: enantiomeric recognition and gas adsorption properties.**